ELSEVIER

Journal of Alloys and Compounds 311 (2000) 143–152

Journal of ALLOYS AND COMPOUNDS

www.elsevier.com/locate/jallcom

# Study of sites occupation and chemical environment of $Eu^{3+}$ in phosphate-silicates oxyapatites by luminescence

L. Boyer[a,*], B. Piriou[b], J. Carpena[a], J.L. Lacout[c]

[a]*Commissariat à l'Energie Atomique de Cadarache, DCC/DESD/SEP/LEMC, Bât 307, 13108 St Paul les Durance, France*
[b]*Laboratoire de Structure, Propriétés et Modélisation du Solide, UMR 8580, Ecole Centrale de Paris, Grande Voie des Vignes, 92295 Châtenay-Malabry Cedex, France*
[c]*CIRIMAT/ENSCT/Laboratoire de Physico-chimie des Phosphates, 38 Rue des 36 Ponts, 31400 Toulouse, France*

Received 27 November 1999; accepted 4 June 2000

**Abstract**

Silicate apatites called britholites have been studied due to their potential application as materials in the form of nuclear waste for the containment of actinides. The luminescence study of $Eu^{3+}$ in the solid solution $Ca_{10-x}La_x(SiO_4)_y(PO_4)_{6-y}O_z\square_{2-z}$ (with $z=1+1/2(x-y)$) allows us to predict the location of an eventual actinide ion and provide structural information on the expected behaviour of the structure towards irradiation damage. The luminescence study confirms the preferential location of the $Eu^{3+}$ ion in the 6*h* site ($C_s$ point symmetry) of the space group $P6_3/m$, where a strong crystal field due to $Eu^{3+}$–O(4) bond occurs. This bond competes with oxygen $SiO_4$ and $PO_4$ tetrahedra and the competing is found to be stronger when silicate groups are present. This is because silicate tetrahedra are less compact than phosphate tetrahedra and are able to approach $Eu^{3+}$ much closer. It is also shown that the crystal field strength decreases with silicate content. The luminescence spectra tend towards those which are more common of $Eu^{3+}$ luminescence in which phosphates are doped with rare earth ions. The spectra of luminescence versus temperature confirms that the crystal field between $Eu^{3+}$(6h)–O(4) is stronger when the temperature is low and the cell parameters are small. 

*Keywords:* Luminescence; X-ray diffraction; Silicate apatite; Trivalent europium; Site-selective spectroscopy

## 1. Introduction

Apatites form a large family of isomorphous compounds with the general chemical formula $Me_{10}(TO_4)_6X_2$, where Me generally represents a divalent cation ($Ca^{2+}$, $Sr^{2+}$, $Pb^{2+}$, $Cd^{2+}$), $TO_4$ a trivalent anionic group ($PO_4^{3-}$, $VO_4^{3-}$, $AsO_4^{3-}$) and X a monovalent anion ($Cl^-$, $F^-$, $OH^-$). A well-known representative member of the apatite group is calcium phosphate fluorapatite $Ca_{10}(PO_4)_6F_2$. Apatites generally crystallise in the hexagonal system (space group $P6_3/m$; $C_{6h}^2$ [1]); the quasi-compact arrangement of the anion groups ($TO_4$) forms the skeleton of the apatite and exhibits two types of channels. The first is occupied by four Me cations (4*f*) with a $C_3$ point symmetry, placed on the ternary axis. The second is occupied, on its periphery, by six cations (6*h*) with $C_s$ site symmetry.

Considerable research effort has therefore been expended on the study of the crystal and solid solution in powder of apatites by medical, biological, earth and nuclear scientists. One of the main characteristics of the apatite structure is that it allows a large number of substitutions at all three sites (Me, T and X). Some of these substitutions can be realised without any change of cationic or anionic charge. For example, hydroxyapatite ($Ca_{10}(PO_4)_6(OH_2)$) is the structural prototype of the main inorganic constituent of bone and teeth, while fluorapatite $Ca_{10}(PO_4)_6F_2$ with its various substituted species, is the principal mineral in commercial phosphate ores. It is also possible to substitute the bivalent cation with a trivalent cation and trivalent anion ($PO_4^{3-}$) with a tetravalent anion ($SiO_4^{4-}$). The mineral obtained through ($Ca^{2+}$, $PO_4^{3-}$)⇔($Ln^{3+}$, $SiO_4^{4-}$) is designated as britholite. In fact, a solid solution exists between phosphate apatite $Ca_{10}(PO_4)_6F_2$ and silicate apatite $Ca_4Ln_6(SiO_4)_6F_2$ (Ln= La, Nd) [2]. Silicate apatites are also found in nature [3]. Natural silicate apatites (rarely containing six silicates) are known to incorporate lanthanides and actinides into their lattice structure. Minerals of the apatite group are characterised by a high resistance to chemical corrosion in neutral to alkaline environments and by their potential for

*Corresponding author.

0925-8388/00/$ – see front matter 
PII: S0925-8388(00)01085-9

restoring self-irradiation damages. This stability of the apatite structure has thus allowed the detection of some britholite in the natural nuclear reactor (Oklo) without corrosion or irradiation damage [4]. Such minerals have been proposed as potential matrices for actinides conditioning [5]. The aim of our study has thus been performed so that these types of minerals can be characterised.

The doped apatites were widely investigated because of their use as fluorescent lamp phosphors and in laser technology. Silicate dioxyapatites are excellent matrices for luminescence of various lanthanides ions. For example, the luminescence of $Eu^{3+}$ in $Me_2Ln_8(SiO_4)_6O_2$ (Me=Mg, Ca; Ln=Y, Gd, La) [6], $Ce^{3+}$ and $Tb^{3+}$ in $Gd_{9,33}(SiO_4)_6O_2$ [7]; $Pr^{3+}$ in $Ba_2La_8(SiO_4)_6O_2$ [8]; $Nd^{3+}$ in $Sr_2La_8(SiO_4)_6O_2$ [9]; $Eu^{3+}$ in $Me_2Y_8(SiO_4)_6O_2$ (Me=Mg, Ca, Sr) [10,11], and $Eu^{3+}$ in $Ca_2Gd_8(SiO_4)_6O_2$ has been investigated.

In the apatite structure ($P6_3/m$ space group), two sites are available for activator cations, 4*f* ($C_3$ point symmetry) with 9-fold coordination and 6*h* ($C_s$ point symmetry) with 7-fold coordination. The large difference between these two sites is that the cation in 6*h* position is coordinated to an O(4) oxygen ion that is present in the channel and is sometimes called 'free oxygen ion'. This oxygen atom does not belong to any silicate group and the binding strength of the O(4) ion is not saturated. The nine oxygen ions coordinated to the 4*f* site all belong to the silicate group. This difference results in the average covalency of the 6*h* site is higher than that of the 4*f* site. Two methods, the variation of the lattice parameters of the apatite with the ionic radius of the constituting lanthanides, and the local charge compensation were utilised by Felsche [12] and Blasse [13], respectively, to study the problem of cation site occupation in these compounds. According to Felsche for the silicate dioxyapatites $Me_2Ln_8(SiO_4)_6O_2$ (Me=Mg, Ca, Sr, Ba; Ln=Lanthanides), the $Mg^{2+}$, $Ca^{2+}$ ions are assumed to be in 6*h*, and $Sr^{2+}$, $Ba^{2+}$ in 4*f*; whereas Blasse proposed that the alkaline-earth metals may be found in 4*f*, except $Ln^{3+}$ ions that are too large (e.g. $La^{3+}$) and $Me^{2+}$ ions which are to small (e.g. $Mg^{2+}$). $Me^{2+}$ ions are also expected to be found in 6*h*. Blasse [13] predicted that by doping these compound with $Eu^{3+}$, the $Eu^{3+}$ ions enter the 6*h* sites in $Me_2La_8(SiO_4)_6O_2$ and 4*f* sites in $Me_2Y_8(SiO_4)_6O_2$ (Me=Mg, Ca), respectively. This is based on the fact that the $Eu^{3+}$ is smaller than $La^{3+}$ and larger than $Y^{3+}$. In later reports [7,8], the doping rare earth ions ($Ce^{3+}$, $Pr^{3+}$) have been found to occupy both the 4*f* and 6*h* sites in $Me_2Y_8(SiO_4)_6O_2$ (Me=Mg, Ca, Sr) by luminescence spectroscopy.

The temperature dependence and the oxygen content dependence in the apatite channel (*z* value in the solid solution $Ca_{10-x}La_x(SiO_4)_y(PO_4)_{6-y}O_z\square_{2-z}$ with $z = 1 + 1/2(x - y)$ and the effect of the phosphate/silicate substitution (*y* value) on the luminescence spectra are described in this paper). Some new results have been obtained. The luminescence study of $Ca_2La_{7.8}Eu_{0.2}(SiO_4)_6O_2$ compound has been carried out in order to determine the spectral lines of known different $Eu^{3+}$ environments. These in turn where then used by comparison to identify new $Eu^{3+}$ environments by a luminescence study of $Eu:Ca_{10-x}La_x(SiO_4)_y(PO_4)_{6-y}O_z\square_{2-z}$ solid solution where the double substitution ($Ca^{2+}$, $PO_4^{3-}$)↔($La^{3+}$, $SiO_4^{4-}$) were made. The luminescence study of the solid solution allows to predict the location of an eventual actinide and later to predict the irradiation damage. The knowledge of the environment of the lanthanide (chemical analogue of trivalent actinide) will allow us to understand the mechanisms responsible for the self restoration of the apatite structure.

## 2. Experimental

### 2.1. Synthesis and characterisation

Powder samples for the series of the solid solution $Eu:Ca_{10-x}La_x(SiO_4)_y(PO_4)_{6-y}O_z\square_{2-z}$ with $z = 1 + 1/2(x - y)$ were prepared by a solid reaction at high temperature (1400°C) for 6 h. The starting materials $CaCO_3$, $SiO_2$, $Ca_2P_2O_7$, $La_2O_3$, $Eu_2O_3$ and reagents used for analysis (PROLABO) were of analytical quality. One of the advantages of this preparation method is the facility of calculation of the weight of the different compounds to obtain the stoichiometry. A preliminary treatment was necessary to obtain well-crystallised apatites. It consists of heat the mixture at 900°C for several h with intermediate grinding. This allows to release $CO_2$ gas that gives a homogeneous mixture.

X-ray diffraction patterns were obtained from powdered samples by using a Siemens D 501 diffractometer ($K\alpha_1$ copper). These confirm that all samples only contain a pure apatite phase which crystallise in the hexagonal system (space group, $P6_3/m$). The IR spectra (Perkin-Elmer FTIR 1600) allow confirmation of the tetrahedral $SiO_4$ and $PO_4$ groups substitution.

### 2.2. Methods

The luminescence studies were performed by time-resolved spectroscopy under selective and non-selective excitations. The measurement were carried out with the third harmonic of a Q-switched neodymium YAG laser (Spectra Physics Quanta Ray, model DCR4), as a non-selective excitation source. This laser was also used to pump a tuneable dye laser (Jobin Yvon, LA04/E1T model) for the site-selective excitation in the $^5D_0$ and $^5D_1$ levels. The spectral analysis of the luminescence was achieved by an 80-cm double grating monochromator (PHO Coderg) spectrometer driven by a computer that collected and processed the data. The time-resolved spectroscopy was performed by means of a digital oscilloscope (Tektronix

2430) coupled with the computer by using home-made programs [14]. Although some measurements were carried out at room temperature or at 77 K by immersion in liquid $N_2$, most of them were done in a helium close-cycle refrigerator at about 20 K (Cryophysics, CP62-STS).

## 3. Results

### *3.1. $Ca_2La_{7.8}Eu_{0.2}(SiO_4)_6O_2$ dioxyapatite*

The time-resolved $^5D_0 > ^7F_{0,1,2}$ emission under UV (355 nm) excitation at 20 K shown in Fig. 1a indicates the contribution of several sites. The broadness of the lines suggest that the sites are continuously distributed. Nevertheless, two kinds of non-equivalent $Eu^{3+}$ sites α and β can be clearly seen under selective excitation in $^5D_0$ level. This is shown in Fig. 1b. The spectrum under selective excitation at 17 299 $cm^{-1}$ (site α), exhibits three lines that can be assigned to the $^5D_0 > ^7F_1$ transitions and four lines that can be attributed to $^5D_0 > ^7F_2$ transitions. The equivalent lines appear for the spectrum of site β under selective excitation at 17 365 $cm^{-1}$ (Fig. 1b). The energy level of the Stark components of the α and β sites are summarised in Table 1.

Despite the selective excitation the lines remain broad due to cationic disorder (Ca and La). For comparison, the spectrum of $Ca_{9.2}Eu_{0.2}(PO_4)_6O\square$ (with sites denoted β′) under 18 108 $cm^{-1}$ excitation ($^5D_1$ level) is given in Fig. 2. The three spectra are similar with an evolution from α to β′ via β. The degeneracy of $^7F_J$ levels are fully lifted and the sites are of low symmetry. Seven lines are clearly seen for the $^5D_0 > ^7F_{1,2}$ transitions of β′ (see Fig. 2) and the sublevels are reported in Table 1. An additional weak and

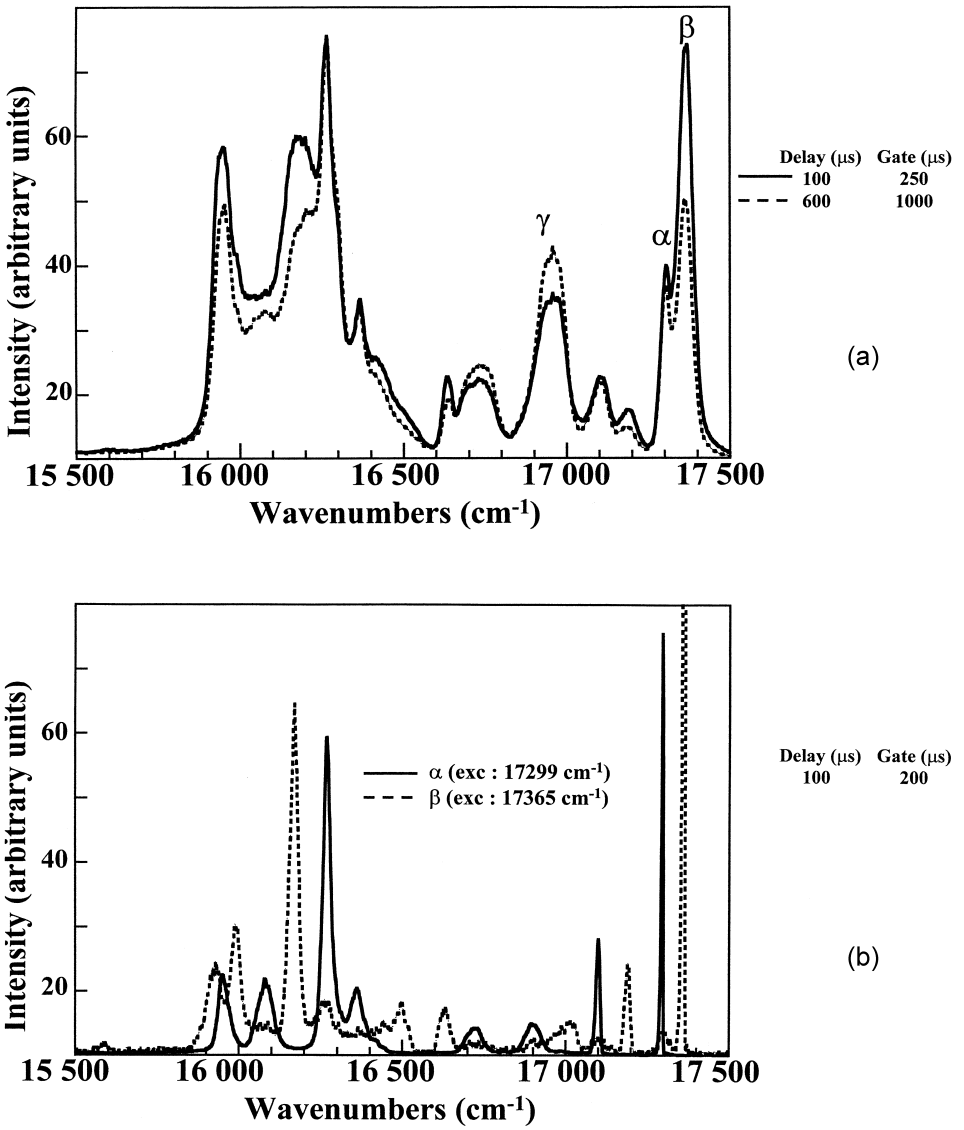


Fig. 1. (a) Time-resolved $^5D_0 > ^7F_{0,1,2}$ emission spectrum of $Ca_2La_{7.8}Eu_{0.2}(SiO_4)_6O_2$ at 20 K under UV (355 nm) excitation. (b) $^5D_0 > ^7F_{0,1,2}$ emission spectra of $Ca_2La_{7.8}Eu_{0.2}(SiO_4)_6O_2$ at 20 K under different excitations (α and β spectra).

Table 1
Energy level of the Stark components ($cm^{-1}$) of α, β and γ sites of $Ca_2La_{7,8}Eu_{0,2}(SiO_4)_6O_2$ at 20 K[a]

| | Levels ($cm^{-1}$) | | | |
|---|---|---|---|---|
| | α | β | β′ | γ |
| $^5D_0$ | 17 299 S | 17 365 S | 17 416 S | 17 250 |
| | 196 | 173 | 161 | 292 |
| $^7F_1$ | 400 | 347 | 300 | 324 |
| | 581 | 724 | 1000 | 498 |
| | 883 | 868 | 761 | 901 |
| | 936 vw | 921 vw | 811 vw | 964 |
| $^7F_2$ | 1026 | 1192 | 1344 | 1052 |
| | 1215 | 1366 | 1500 | 1080 |
| | 1343 | 1441 | 1522 | 1290 |

[a] β′ site belongs to $Ca_{9.2}Eu_{0.2}(PO_4)_6O$ and the assignment is in accordance to the study of Voronko et al. [16] in $Eu:Ca_{10}(PO_4)_6F_2$ single crystal. vw, very weak; S, strong corresponding line.

broad line at about 16 420 $cm^{-1}$ must not be neglected. Its occurrence is confirmed by similar spectra in which this line is much more resolved, such spectra were reported in phosphate apatites [15–18] and in other types of compounds where an Eu–O bond was assumed [19–22]. By comparison to the polarised luminescence study of $Eu:Ca_{10}(PO_4)_6F_2$ single crystal by Voronko et al. [16], this line has been ascribed to $^5D_0 > ^7F_1$ transitions of the highest $^7F_1$ manifold. Such an assignment involve a very high value of the Stark splitting of the $^7F_1$ level: 839 $cm^{-1}$ for β′ site and up to 997 $cm^{-1}$ in calcium fluorapatite [16]. This leads to an overlap of the manifolds of the $^7F_1$ and $^7F_2$ levels (Fig. 2). What is unusual about the β and β′ spectra attained, is also the positioning of the $^5D_0$ level and the intensity of the $^5D_0 > ^7F_0$ forbidden line. For the β′ site the relation between the intensities related to the surfaces of the $^5D_0 > ^7F_0$ transition and all lines of the $^5D_0 > ^7F_J$ transitions are $I(^5D_0 > ^7F_0)/I(^5D_0 > ^7F_1) \approx 12.3$ and $I(^5D_0 > ^7F_0)/I(^5D_0 > ^7F_2) \approx 1.2$. The decay corresponding to $^5D_0$ are nearly exponential. At 20 K, the life times are: 1.14 ms, 907 μs and 500 μs for, α, β and β′, respectively. In the last case the life time is particularly short for the $^5D_0$ level of $Eu^{3+}$ in an oxide compound.

### 3.1.1. Fluorescence line narrowing

As previously noted, the α and β sites belong to a distribution of which the $^5D_0 > ^7F_0$ transition lines lie between 17 250 and 17 440 $cm^{-1}$. This inhomogeneous line was investigated by the $^5D_0 > ^7F_{1,2}$ emission spectra under $^5D_0$ level selective excitations with a step of 10 $cm^{-1}$. The important splitting for $^7F_1$ and $^7F_2$ levels increase as that of the $^5D_0$ levels increase (Fig. 3). In this figure it can be seen that the shift of these sublevels uniformly varies, except for two lines. A small jump and superposition occurs for $^5D_0$ in the 17 310–17 330-$cm^{-1}$ range.

### 3.1.2. Excitation spectra in the $^5D_1$ level

To verify the continuity of the α/β distribution, the shift of the $^5D_1$ components versus the $^5D_0$ level was followed by their excitation spectra. Except for some low $^5D_0$ levels, within the range 17 250–17 440 $cm^{-1}$, three well-separated lines can be observed (Fig. 4a). Here their continuous shift (Fig. 4b) indicates a wide distribution of the sites for $^5D_0$ level between 17 300 and 17 365 $cm^{-1}$ (sites α and β) and beyond. Their splitting increases as $^5D_0$ level and are in coherence with $^7F_1$ splitting.

For $^5D_0$ level close to 17 265 $cm^{-1}$ the excitation spectra reveal the occurrence of another site out of the distribution, labelled γ, characterised by only two $^5D_1$ components and by a longer life time, about 2.5 ms (Fig. 4a,b). Under selective $^5D_1$ excitation at 19 800 $cm^{-1}$ the site γ is also well characterised by its $^5D_0 > ^7F_{0,1,2}$

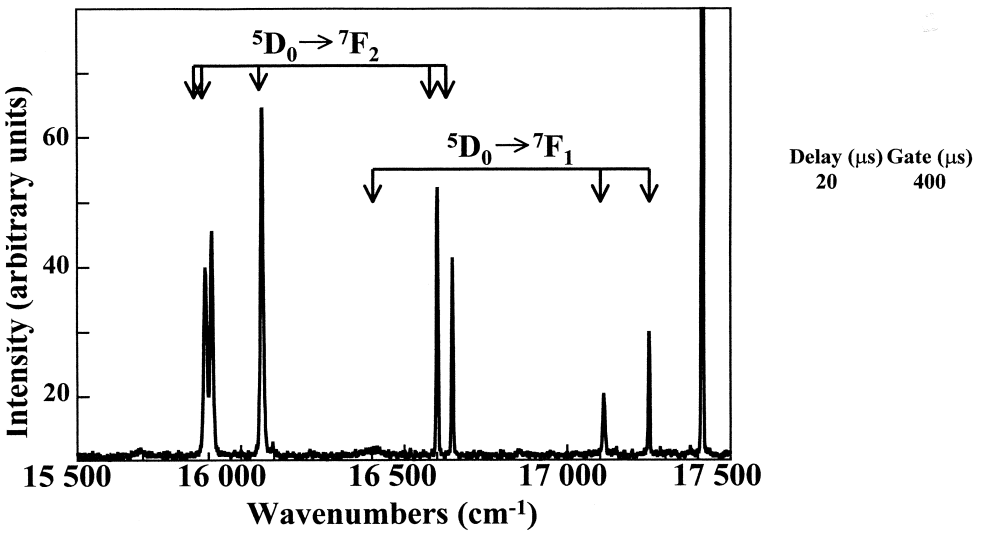


Fig. 2. $^5D_0 > ^7F_{0,1,2}$ emission of $Ca_{9,2}Eu_{0,2}(PO_4)_6O\square$ at 20 K under selective excitations of 18 108 $cm^{-1}$ (β′ spectrum).

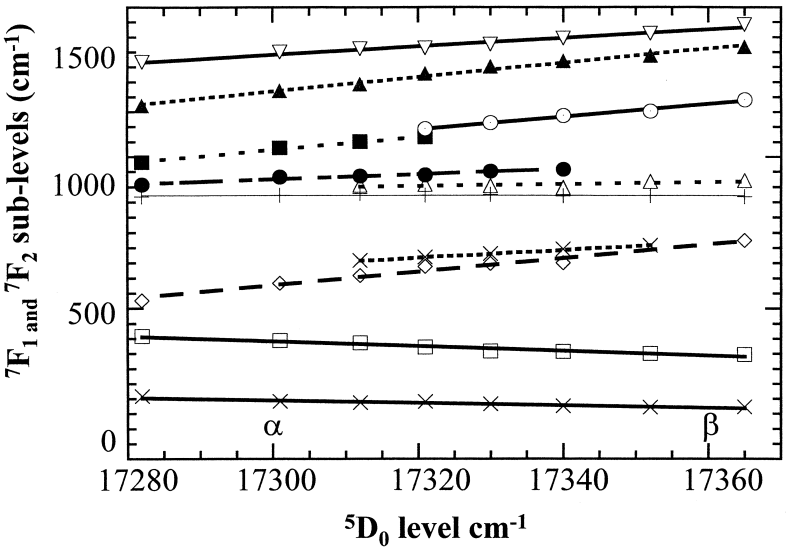


Fig. 3. Energy of the $^7F_1$ and $^7F_2$ sub-levels of $Eu^{3+}$ in $Ca_2La_{7,8}Eu_{0,2}(SiO_4)_6O_2$ at 20 K versus the $^5D_0$ level.

emission spectrum (Fig. 5). Contrary to the other sites one can point out the weakness of its $^5D_0 > ^7F_0$ line. As seen previously under UV (Fig. 1a) the contribution of this longer decay time site increases at long delay in the time resolved spectra (line at 16 700 and 16 940 $cm^{-1}$). No one secondary phase has been detected by IR spectra or RX diffraction. This third optical environment of the $Eu^{3+}$ ion is considered to belong to the apatite structure too.

### *3.1.3. Temperature dependence*

During the cooling of the sample, the intensity of the luminescence strongly increased and the profile changed as shown in Fig. 6a. As the temperature decreases the intensity of the $^5D_0 > ^7F_0$ line of the site β increases more rapidly than that of the site α (Fig. 6b).

### *3.2. Luminescence of the solid solution $Eu:Ca_{10-x}La_x(SiO_4)_y(PO_4)_{6-y}O_z\square_{2-z}$ ($z=1+1/2(x-y)$)*

### *3.2.1. Cationic substitutions and oxygen content in the silicate apatites ($y=6$)*

In the solid solution $Eu:Ca_{10-x}La_x(SiO_4)_y(PO_4)_{6-y}O_z\square_{2-z}$, one considered two members, the oxysilicate apatite for $x=5.8$ ($Ca_4La_{5.8}Eu_{0.2}(SiO_4)_6O\square$) and the dioxysilicate apatite for $x=7.8$ ($Ca_2La_{7.8}Eu_{0.2}(SiO_4)_6O_2$) already seen in Section 3.1. Their $^5D_0 > ^7F_{0,1,2}$ emission spectra (Fig. 7 and Fig. 1a) under UV excitation are similar. The main difference is the α/β emission ratio. The contribution of the β site is lower for the oxysilicate apatite than for the dioxysilicate apatite.

### *3.2.2. $PO_4/SiO_4$ ratio dependence*

In the solid solution $Eu:Ca_{10-x}La_x(SiO_4)_y(PO_4)_{6-y}O_z\square_{2-z}$, under non selective excitation at 355 nm (Fig. 8) the luminescence seems to correspond to the superposition of the emission of several centres, such as α, β sites and even γ site in the case of the end member ($x=5.8$), the oxysilicate apatite. With increasing group content of silicate the intensity of the $^5D_0 > ^7F_0$ lines decrease and their position shift towards lower frequency. By using the site selective excitation of the oxysilicate apatite at 17 300 and 17 365 $cm^{-1}$ it was possible to attain separately the $^5D_0 > ^7F_{1,2}$ emission of α and β, as for the dioxysilicate apatite seen previously (Fig. 1b).

## 4. Discussion

Despite its strong $^5D_0 > ^7F_0$ line and its rather large $^7F_1$ splitting, the α site exhibits a nearly regular spectroscopic behaviour for the $Eu^{3+}$ ion. However, contrary to this non-conventional spectra of β and β′ sites are similar to those encountered in phosphate apatites [15–18]. Such peculiar spectra were also encountered for $Eu^{3+}$-doped cordierite and some silicates prepared by the sol–gel route [19,20]. The unusual spectra features are mainly the following.

- The high energy of $^5D_0$, $^5D_1$ and $^5D_2$ levels.
- The very large $^7F_J$ splitting. The $^7F_1$ and $^7F_2$ manifolds overlap and lines appear in vicinity of 16 500 $cm^{-1}$, range usually free of lines.
- A peak of high intensity that corresponds to the forbidden $^5D_0 > ^7F_0$ transition.
- The short $^5D_0$ life time, 780 μs for the β site of the distribution which have the highest $^5D_0$ level (17 365 $cm^{-1}$).

Many problems arise for spectral interpretation. As far

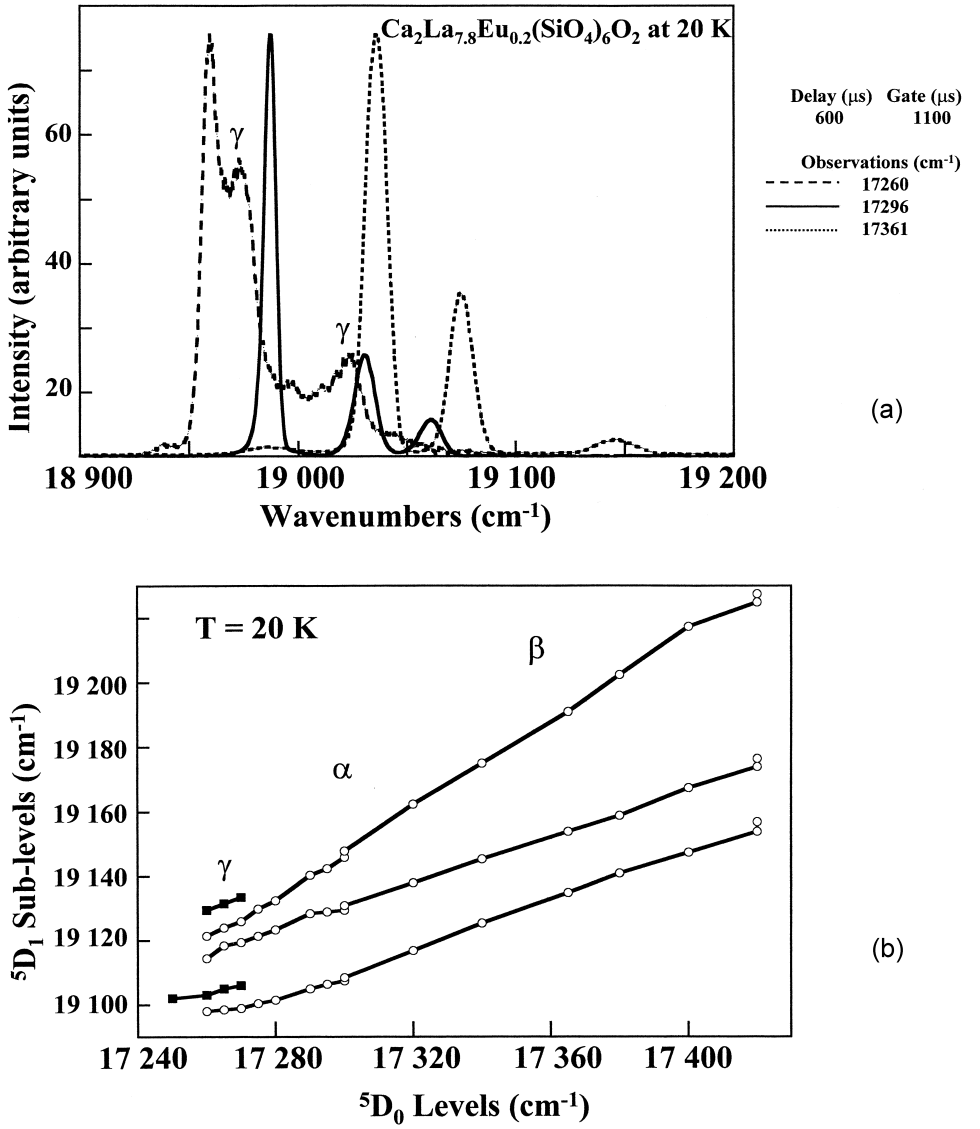


Fig. 4. (a) $^5D_1$ excitation spectra of α/β site distribution (doted and full lines) and γ site (dashed line). (b) Energy of the $^5D_1$ components versus the $^5D_0$ level at 20 K of the sites in dioxysilicate apatite.

as we know, such data have not been reported, except for particular apatite structures. In the compound Eu:$Y_6WO_{12}$, in which one distance Y–O is clearly shorter than the another (2.12 instead 2.27 Å and more), an important $^7F_1$ splitting (553 $cm^{-1}$) occurred [23]. It is comparable to the one of the β site (551 $cm^{-1}$), but it remains weak with respect to that of the β′ site (839 $cm^{-1}$). Concerning the intensity of the $^5D_0 > ^7F_0$ transition, the highest values appearing in the literature ($I(^5D_0 > ^7F_0)/I(^5D_0 > ^7F_2)$= 0.48 and 0.45 for Eu:$Sr_2TiO_4$ and Eu:$Ba_3Gd_2WO_9$ [24] are about half of our observation data (1.2)). The abnormal behaviour of $Eu^{3+}$ in apatites has been discussed in the cited literature. More generally the laser technology reaps the advantage of the rare-earth ions in the vanadate apatite matrix [25]. In the framework of the Judd–Ofelt theory the features pointed out above were explained in terms of a strong anisotropic crystal field. The high values of the crystal field parameters should induce a strong *J*-mixing within the $4f^6$ configuration and a strong mixing of the $4f^6$ and $4f^5 5d^1$ electronic configuration. On this basis, the crystal field analysis to calculate the energy of the $^7F_1$ and $^7F_2$ manifolds of Eu:$Sr_{10}(PO_4)_6F_2$ fails [26], nevertheless an unusually important *J*-mixing of $^7F_J$ was found.

It seems that such considerations cannot account for the spectral features of $Eu^{3+}$ in the apatite structure, in peculiar the intensity of the $^5D_0 > ^7F_0$ transition. One might find an explanation by using the pseudo-multipolar field when the *J*-mixing is included [27]. An enhancement of the $^5D_0 > ^7F_0$ and of $^5D_0 > ^7F_2$ transitions and their ratio $I(^5D_0 > ^7F_0)/I(^5D_0 > ^7F_2)$ is expected, but in the case of the apatites such intensity have not been evaluated yet.

As it was suggested in an earlier paper [15] the covalence degree of a privileged Eu–O(4) bond should be responsible for such effects which increase when the

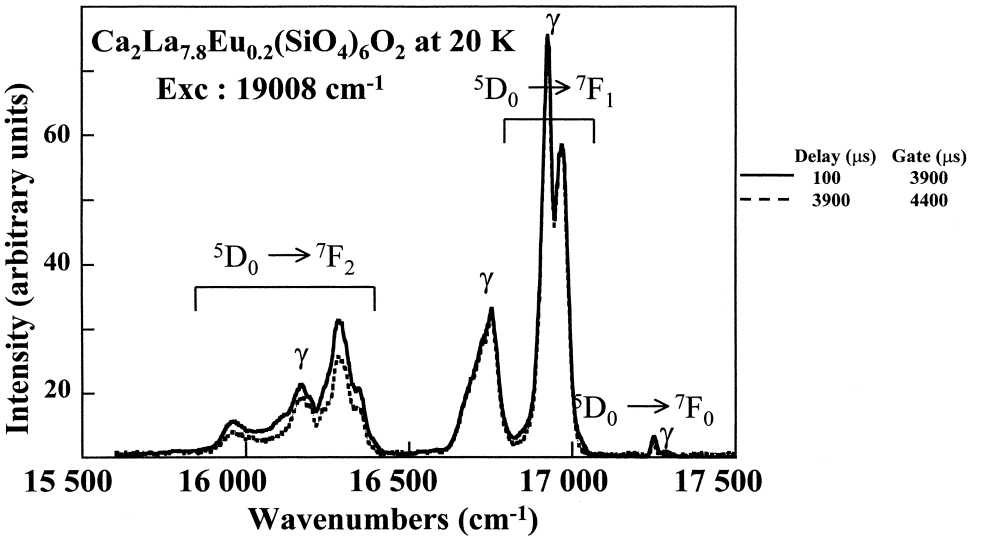


Fig. 5. $^5D_0 > {}^7F_{0,1,2}$ emissions spectrum of the γ site under excitation in the $^5D_2$ level.

distance is short. The covalent effect was evaluated in the case of $Pr^{3+}$ ion [28]. It has been shown that one cannot neglect an additional source of electric dipole transition intensity due to the overlap of the 6p orbital with the oxygen 2p orbital. Unfortunately this mechanism was not applied to $Eu^{3+}$.

The preferential occupation of $Ln^{3+}$ ion in 6*h* position of an apatite structure was widely described in literature [10,11,13,15,29–31]. A Ln–O bond was evidenced by a localised vibration by using both IR spectroscopy [32,33], and Raman scattering [15]. Despite an assumed rigorous $C_s$ point symmetry for 6*h* position a pseudo $C_{\infty v}$ symmetry along the Eu–O bond well agrees with the data indicating that the double degeneracy of three components is slightly lifted into doublet (β′ spectra).

The investigated silicate–phosphate apatites present a continuous broad distribution of sites from α to β, and beyond. This is shown by the shift of $^7F_1$, $^7F_2$ and $^5D_1$ manifolds as a function of the $^5D_0$ level. The continuity is probably due to the different geometric arrangements of both the cationic environment ($Ca^{2+}$, $La^{3+}$ and $Eu^{3+}$) and the anionic environment. In this disordered structure the distance Eu–O(4) can uniformly change but two more probable distances should explain the occurrence of the two prominents α and β sites within the distribution.

In the silicate apatites $Ca_{10-x}La_{x-0.2}Eu_{0.2}(SiO_4)_6O_{x/2-2}\square_{4-x/2}$ the relative occurrence of the β and α sites seems depend on the oxygen content (Figs. 1a and 7). Their ratio β/α, related to the intensity of the $^5D_0 > {}^7F_0$ line, is greater for the dioxysilicate apatite than for the oxysilicate apatite. This means that the short Eu–O(4) bond lengths are favoured by the amount of oxygen atoms in the channel. Indeed the presence of vacancies induces an electrostatic disorder which is minimised by the position of the O(4) atoms. The oxygen is shifted of the m mirror toward the nearest vacancy [34]. The Eu–O(4) distance is increased and consequently reduces the covalent character of the bond.

The Eu–O(4) distance also depends on the channel size. At first, at low temperature the cell parameters are smaller than those at room temperature and the $Eu^{3+}$–O(4) bond lengths are shorter. Furthermore, at low temperature, thermal agitation is minimised and consequently the O(4) is stabilised when in close approximation to $Eu^{3+}$. This explains the thermal dependence of the ratio $I_\beta/I_\alpha$. Secondly, the $PO_4$ content also plays a role. The volume of the silicate tetrahedra is more important than the volume of phosphate tetrahedra. The mean bond lengths are Si–O = 1,62 Å and P–O = 1.548 Å [34]. Consequently, in britholite $Ca_2La_{7.8}Eu_{0.2}(SiO_4)_6O_2$, the oxygen atoms of tetrahedra are closer to $Eu^{3+}$ in 6*h* position. For the phosphate–silicate apatite the abnormal high intensity of the line that corresponds to the $^5D_0 > {}^7F_0$ transition (site β), reveals a strong crystal field that is correlative with the $PO_4$ content (Fig. 8). In fact, the $SiO_4$ tetrahedra are less rigid and the oxygen polyhedra are more bonding to $Eu^{3+}$ in the case of pure silicate apatite than pure phosphate apatite. As this ionic bonding is in competition with the covalent bonding Eu–O(4), the characteristic bond Eu–O(4) in the apatite structure containing more silicate, is the least covalent. Consequently, for phosphate apatite a greater crystal field is obtained between $Eu^{3+}$(6*h*)–O(4) than for phosphate–silicate apatite and the spectral line attributed to $^5D_0 > {}^7F_0$ appears at a higher frequency with a greater intensity.

The short $^5D_0$ level life time of the β′ site (0.5 ms), can be understood as a non-radiative de-activation by the vibration localised on the Eu–O bond. To corroborate the significant influence of a covalent Eu–O bond on the exceptional optical properties of $Eu^{3+}$, one must note that the observed spectra are not characteristic of the apatite structure but to this particular bond. Indeed, quite similar spectra appear in fluoride compounds in which the residual

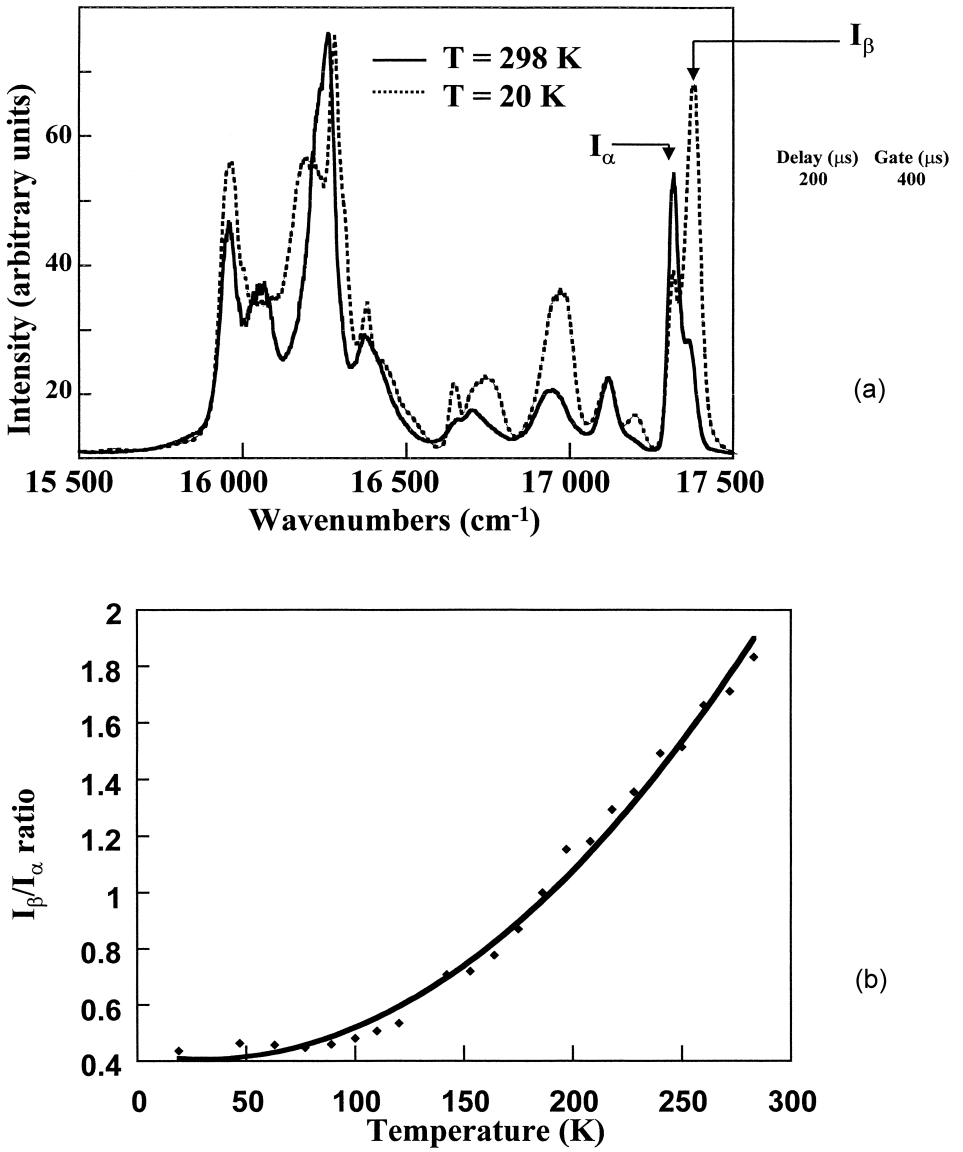


Fig. 6. (a) Temperature dependence of the $^5D_0 > ^7F_{0,1,2}$ emission of $Ca_2La_{7,8}Eu_{0,2}(SiO_4)_6O_2$ under UV (355 nm) excitation. (b) Temperature dependence of the $I_\beta/I_\alpha$ ratio intensity of the $^5D_0 > ^7F_0$ line of the two sites.

oxygen cannot be totally avoided (Eu:$RbCaF_3$ [21] and Eu:$KGdF_7$ [22]). In the same way, for Eu:α-$Mg_2Al_4Si_5O_{18}$ [20] and for some $Eu^{3+}$-doped silicates [19] parent spectra were reported.

In the $Ca_2La_8(SiO_4)_6O_2$ which was more investigated thoroughly a third site γ was observed, although less distributed. Such a site is unknown in literature. These data show that the site γ does not belong to the broad distribution (Fig. 4b). This means that γ is characteristic of another crystallographic site than α/β sites. When a $Eu^{3+}$ ion is located in an inversion centre site the electric dipole transitions are forbidden. The radiative de-activation processes are limited only to the magnetic dipole transitions, this can increase the life time of the levels. Thus, the life time of the $^5D_0$ level is 7.7 ms for the $C_{3i}$ site for $Eu^{3+}$ in $Y_2O_3$ [35] and 9 ms for the same point symmetry $C_{3i}$ in calcite [36]. Consequently, the long life time of the γ site, 2.5 ms instead of about 1 ms that is usually observed for the oxide compound, indicates a symmetrical neighbouring of this site. Further indication of this is also given by the weak intensity of the $^5D_0 > ^7F_{0,2}$ electric dipole transition with respect to the $^5D_0 > ^7F_1$ magnetic dipole transition. On the other hand, the number of the observed transitions (two lines for $^5F_0 > ^5D_1$ transition, one line and one doublet for $^5D_0 > ^7F_1$ transition and only three lines for $^5D_0 > ^7F_2$ transition) agree with a site symmetry close to an axial symmetry. In a first approach the 4*f* position of $C_3$ point symmetry could satisfy all spectral requirement for

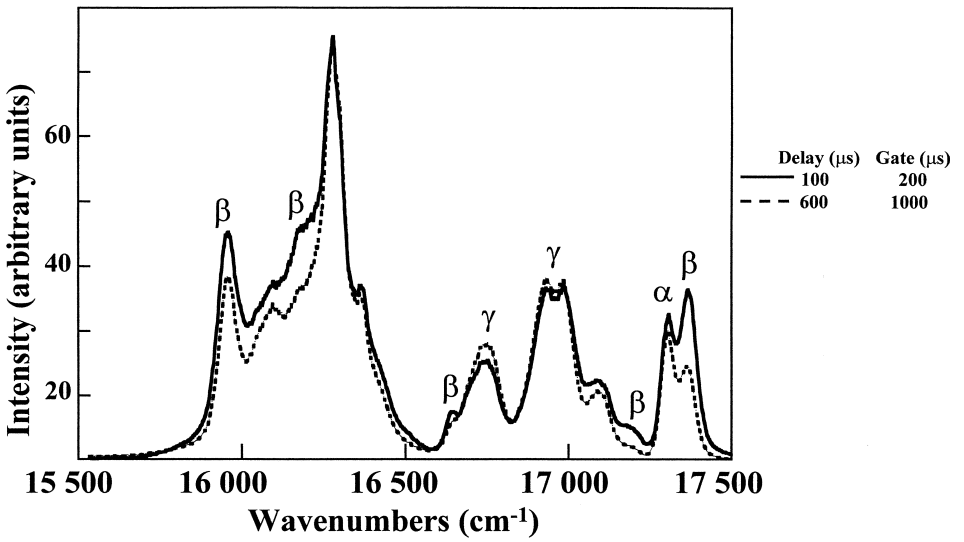


Fig. 7. Time-resolved $^5D_0 > {}^7F_{0,1,2}$ emission spectrum of oxyapatite $Ca_4La_{5,8}Eu_{0,2}(SiO_4)_6O\square$ at 70 K under UV (355 nm) excitation.

the γ site. In the oxyapatites the occupation rate of $Eu^{3+}$ ion in this position increase as the ratio $SiO_4/PO_4$ increases (Fig. 8).

## 5. Conclusion

The luminescence study of the solid solution Eu: $Ca_{10-x}La_x(SiO_4)_Y(PO_4)_{6-Y}O_Z\#_{2-Z}$ where $Z=1+1/2(X-Y)$ indicates that both the 6*h* and 4*f* sites apatite structure are occupied by $Eu^{3+}$ and therefore by $La^{3+}$. The lanthanide ion shows a strong preference for the 6*h* site that is nearest to the channel containing free oxygen O(4). This site is characterised by the (covalent or ionic) chemical bond nature. The position and the intensity of the characteristic lines of the $^5D_0 > {}^7F_{0,1,2}$ transitions that correspond to the site γ ($Eu^{3+}$ in 4*f* position) are regular. In opposite to the uncommon spectral features of the distributed sites located close to the 6*h* position. The spectral anomalies are understood as a consequence of the covalency of the Eu–O(4) bond. The use of $Eu^{3+}$ as a local probe in the silicate–phosphate solid solution has revealed that the degree of covalency of this Eu–O(4) bond is stronger when neighbouring phosphate groups are

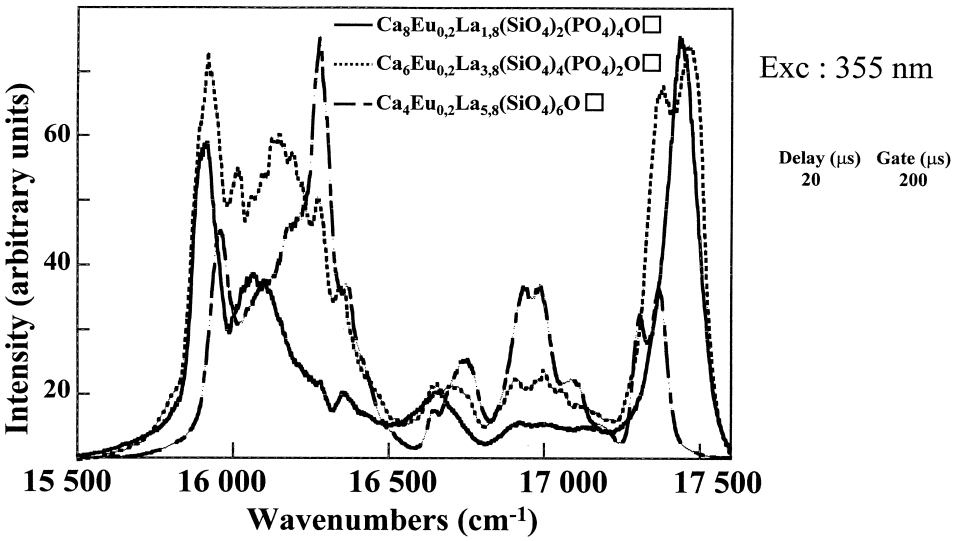


Fig. 8. $^5D_0 \rightarrow {}^7F_{0,1,2}$ emission of $Ca_{9.8-x}Eu_{0.2}La_x(SiO_4)_{0,2+x}(PO_4)_{5.8-x}O\square$ solid solution at 77 K under 355 nm excitation.

present in the apatite than when it is silicate. This can be explained with regards to the phosphate and silicate oxygens' tendency to compete with the $Eu^{3+}(6h)$–O(4) bond in the apatite structure, where that of silicate is greater than phosphate. The stronger the competitiveness, the greater the interaction with $Eu^{3+}$ and therefore the greater the covalent character of $Eu^{3+}(6h)$–O(4). This may be interpreted as a consequence of the greater rigidity of the orthophosphate.

## Acknowledgements

We are grateful to M.D. Faucher for fruitful discussions.

## References

[1] K. Sudarsanan, R.A. Young, Acta Crystallogr. B25 (8) (1969) 1534.
[2] L. Boyer, J. Carpéna, J.L. Lacout, Solid State Ionics, Diffusion Reactions 95 (1,2) (1997) 121–129.
[3] K. Ouzegane, Thesis, Université de Paris VI, 1987, pp. 87–27.
[4] R. Bros, J. Carpéna, V. Sère, A. Beltritti, Radiochim. Acta 74 (1996) 277–282.
[5] J. Carpéna, J.L. Lacout, French Patent, 1993, no. 93 08676.
[6] T.J. Issacs, J. Electrochem. Soc. 120 (1973) 654.
[7] M.J. Lammers, G. Blasse, J. Electrochem. Soc. 134 (1987) 2068.
[8] J.P.M. Van Vliet, G. Blasse, Mater. Res. Bull. 25 (1990) 391.
[9] R.H. Hopkins, G.W. Roland, K.B. Steinbruegge, W.D. Partlow, J. Electrochem. Soc. 118 (1971) 637.
[10] J. Lin, Q. Su, J. Alloys Comp. 210 (1994) 159–163.
[11] J. Lin, Q. Su, Mater. Chem. Phys. 38 (1994) 98–101.
[12] J. Felsche, J. Solid State Chem. 5 (1972) 266–275.
[13] G. Blasse, J. Solid State Chem. 14 (1975) 181–184.
[14] B. Piriou, J. Dexpert-Ghys, S. Mochizuki, J. Phys.: Condens. Matter. 6 (1994) 7317.
[15] B. Piriou, D. Fahmi, J. Dexpert-Ghys, A. Taitai, J. Lacout, J. Luminesc. 39 (1987) 97–103.
[16] Y.K. Voronko, G.V. Maksimova, A.A. Sobol, Opt. Spectrosc. 70 (1991) 203–206.
[17] R. El Ouenzerfi, N. Kbir-Ariguib, M. Trabelsi-Ayedi, B. Piriou, J. Luminesc. 85 (1999) 71–77.
[18] B. Piriou, A, Elfakir, M. Quarton (to be published).
[19] B. Piriou, M. Richard-Plouet, J. Parmentier, F. Ferey, S. Vilminot, J. Alloys Comp. 262–263 (1997) 450–453.
[20] B. Piriou, Y.F. Chen, S. Vilminot, J. Solid State Inorg. Chem. 35 (1998) 341–355.
[21] D. Van der Voort, G. Blasse, J. Phys. Chem. Solids 53 (1992) 219–225.
[22] A. Pierrard, P. Gredin, N. Dupont, A. de Kosak, B. Piriou, J. Alloys Comp. 289 (1999) 71–80.
[23] O. Beaury, M. Faucher, P. Caro, Mater. Res. Bull. 13 (1978) 175–185.
[24] W.C. Nieuwpoort, G. Blasse, Solid State Commun. 4 (1966) 227.
[25] L.D. De Loach, S.A. Payne, B.H.T. Chai, G. Loutts, Appl. Phys. Lett. 65 (1994) 1208–1210.
[26] A.O. Wright, M.D. Seltzer, J.B. Gruber, B.H.T. Chai, J. Appl. Phys. 78 (4) (1995) 2456–2467.
[27] O.L. Malta, Mol. Phys. 42 (1981) 165–172.
[28] M.D. Faucher, O.K. Moune, Phys. Rev. A55 (1997) 4150–4154.
[29] A. Zounani, D. Zambon, J.C. Cousseins, J. Alloys Comp. 188 (1992) 82–86.
[30] R. Jagannathan, M. Kottaisamy, J. Phys. Condens. Matter. 7 (1995).
[31] J.B. Gruber, C.A. Morrison, M.D. Seltzer, A.O. Wright, M.P. Nadler, T.H. Allik, J.A. Hutchinson, B.H.T. Chai, J. Appl. Phys. 79 (3) (1996) 1746–1758.
[32] A. Taitai, J.-L. Lacout, G. Bonel, Ann. Chim. Fr. 10 (1985) 29–35.
[33] L.D. Deloach, S.A. Payne, W.L. Kway, J.B. Tassano, S.N. Dixit, W.F. Kruoke, J. Luminesc. 62 (1994) 85–94.
[34] L. Boyer, J.M. Savariault, J. Carpéna, J.L. Lacout, Acta Crystallogr. C54 (1998) 1057–1059.
[35] J. Heber, K.H. Hellewege, U. Köbler, Murmann, Z. Phys. 237 (189) (1970) 8453–8466.
[36] B. Piriou, M. Fedoroff, J. Jeanjean, L. Bercis, J. Colloid Interface Sci. 194 (1997) 440.